Journal of Applied Electrochemistry (2005) 35:871–878
DOI 10.1007/s10800-005-4738-1

Proton diffusion in γ-manganese dioxide

G.J. BROWNING and S.W. DONNE*
Discipline of Chemistry, University of Newcastle, Callaghan, NSW 2308, Australia
*(*author for correspondence, e-mail: scott.donne@newcastle.edu.au)*

Received 24 September 2004; accepted in revised form 03 March 2005

Key words: electrolytic manganese dioxide, proton diffusion, step potential electrochemical spectroscopy

Abstract

Deconvolution of the electrolytic manganese dioxide (EMD) discharge curve has indicated the presence of a number of energetically different reduction processes. This has been used to determine the contribution of each reduction process to the total discharge. Using step potential electrochemical spectroscopy (SPECS), the i-t data were modelled as the sum of the discharge of the individual reduction processes. From this, $A\sqrt{D}$ for each reduction process as a function of degree of discharge was determined. The maximum $A\sqrt{D}$ values for each process ranged from 2.3×10^{-2} to 4.0×10^{-4} cm^3 s$^{-1/2}$ g^{-1} values are consistent with previously reported values for $A\sqrt{D}$, although in this case we have determined values for the entire compositional range.

1. Introduction

There are numerous primary and secondary battery systems currently available to the consumer. Those that employ the alkaline Zn/MnO_2 chemistry are extremely popular, due mainly to the various advantageous physico-chemical and electrochemical properties of the alkaline manganese dioxide electrode. Despite this consumer popularity, and the extensive research efforts that have gone into understanding this electrode system to date, much of the fundamental understanding of the alkaline manganese dioxide electrode remains unclear, due primarily to the extremely complex interplay between material structure and electrochemical behaviour.

Manganese dioxide can exist in many structural forms [1–3], although the basic building block for all of these is the $[Mn(O^{2-},OH^-,H_2O)_6]^{z+}$ octahedral unit which can be arranged during synthesis to form a range of tunnel or layered structures. Two of the more basic structural varieties are those of pyrolusite (β-MnO_2) and ramsdellite, which are tunnel structures in which the tunnel size is either 1×1 or 1×2 octahedral units. While these are idealized material structures, in reality it is quite common to encounter manganese dioxide samples that are intergrowths between the more basic structures. One such example is that of γ-MnO_2, which in general terms can be considered as a microscopic random intergrowth between the ramsdellite and pyrolusite forms [4]. Additional structural complexity in γ-MnO_2 arises as a result of the presence of partially reduced manganese ions (Mn^{3+} instead of Mn^{4+}), cation vacancies, structural water [5–7] and microtwinning [8], the presence of which is still a matter for debate [9]. γ-MnO_2 is the form used in the alkaline manganese dioxide cathode.

In an aqueous alkaline environment γ-MnO_2 is widely [8, 10–17] believed to reduce via proton and electron insertion into the structure; i.e.,

$$MnOOH_r + \Delta H_2O + \Delta e^- \leftrightarrow MnOOH_{r+\Delta} + \Delta OH^- \quad (1)$$

where r corresponds to the mole fraction of hydrogen (H^+/e^- pair) in the starting material (r is ~0.1 in a typical unreduced γ-MnO_2) and Δ is the added extent of reduction. The extent to which this solid state intercalation process occurs has been found dependent on the alkaline electrolyte concentration [18]. In concentrated electrolytes (e.g., 9 M KOH) solid state reduction occurs until $r + \Delta \approx 0.8$, at which time Mn(III) dissolution can occur [16, 18]. In less concentrated electrolytes solid state reduction can occur for the entire discharge; i.e., $r + \Delta \approx 1.0$ [18].

As indicated in Equation (1), the proton originates from decomposition of a water molecule at the manganese dioxide/electrolyte interface, while the electron comes from the external circuit and enters the manganese dioxide particle via the conductive network in the electrode. The activity gradient thus established between the surface and bulk of the manganese dioxide particle provides the driving force for mass transport which ultimately leads to the protons and electrons being distributed uniformly throughout each particle. Experiments [19] have demonstrated that proton diffusion through the γ-MnO_2 structure is rate limiting, compared to electronic diffusion, for the majority of discharge; i.e., $r + \Delta < 0.8$ in Equation (1).

While this reduction process may seem straightforward, it is complicated substantially by the inherent structural complexity of the γ-MnO_2, as mentioned above. This has been demonstrated in a number of previous studies into the electrochemical behaviour of the manganese dioxide electrode, where the authors have identified a number of reduction processes which they have variously ascribed to the reduction of Mn(IV) ions in surface sites, near defect sites, ramsdellite domains and pyrolusite domains [8, 15–17, 20–22]. While confirmation of these assignments needs to be made, these structural variations influence the rate at which mass transport through the structure can occur.

There have also been numerous studies reported in the literature focused on mass transport within the manganese dioxide electrode. These studies have used a variety of characterization techniques from conventional electrochemical methods such as chronoamperometry [24], chronopotentiometry [23–25] and impedance spectroscopy [26], to various chemical techniques including leaching studies [27], isotope exchange [28], and nuclear magnetic resonance spectroscopy [29]. In all of these, the objective was to extract a diffusion coefficient for mass transport (D), or the term $A\sqrt{D}$, where A is the electrochemically active surface area. For all of these experimental efforts, only one has reported the diffusion coefficient as a function of depth of discharge [23], and no research efforts have been reported where a variety of structurally different γ-MnO_2 samples have been examined.

As a result of these studies, diffusion coefficients for proton transport in manganese dioxide have been reported to range from 10^{-8} to 10^{-19} cm^2 s^{-1} [30]. Clearly with this level of variation, no one experimental method can be identified as a superior technique, nor can the absolute diffusion coefficient be determined. However, if each of these diffusion coefficients are combined with the surface area used in their respective analysis, then irrespective of the technique, the resultant $A\sqrt{D}$ values all fall within an order of magnitude of 10^{-3} cm^3 $s^{-1/2}$ g^{-1} [30]. These two observations clearly indicate that the choice of electrochemically active surface area almost totally accounts for the variation observed in the quoted D values. Two general approaches are apparent in the literature when selecting an appropriate surface area; i.e., either (i) the BET surface area, taking into account the surface area associated with pores accessible to the adsorbate, or (ii) the geometric surface area, based essentially on the macroscopic particle geometry. In reality, the true electrochemically active surface area probably lies somewhere between these two extremes; however, the precise contribution from each is yet to be determined.

Another important point about the reported (or calculated from literature work) $A\sqrt{D}$ values is that while they are more consistent, they reflect only the kinetic behaviour of the starting γ-MnO_2. As mentioned above, there is no indication in the literature as to how $A\sqrt{D}$ varies with degree of discharge, and consequently whether either or both A and D change as a function of discharge. In this work we make use of data from a combination of electrochemical techniques (step potential electrochemical spectroscopy and linear sweep voltammetry) to extract kinetic $A\sqrt{D}$ data for the various processes occurring during γ-MnO_2 reduction.

2. Experimental

2.1. *Sample description*

The starting γ-MnO_2 used in this work was a commercial electrolytic manganese dioxide (EMD) provided by Delta EMD Australia, Pty Limited. It was prepared by electrolysis of a hot ($\sim$98 °C), acidic solution of $MnSO_4$ (acid to Mn molar ratio $\sim$0.4), resulting in deposition of the EMD onto a titanium anode. Following deposition, the EMD was mechanically removed from the anode, milled to a -105 μm powder, neutralized and washed to remove any entrained electrolyte, and then dried at $\sim$ 110 °C before being ready for use. Using standard analytical techniques [5, 31, 32], the O/Mn ratio of this sample was determined to be 1.96 with a surface water content of 1.72%, and the BET surface area using N_2 as the adsorbate at 77 K was 32 m^2 g^{-1}.

2.2. *Electrochemical cell preparation*

The working electrode was prepared by lightly grinding together the manganese dioxide sample (0.200 g), Timcal SFG6 graphite (2.000 g) and 37 wt% KOH (0.370 g) using a mortar and pestle. After 5 min of mixing, the composite was stored in an airtight container overnight to equilibrate before being used.

The electrochemical cell used is shown schematically in Figure 1. Cell assembly involved placing the amount of sample mixture corresponding to 0.020 g of manganese dioxide into a Teflon-lined C-size battery can. The sides of the Teflon sleeve were brushed down to

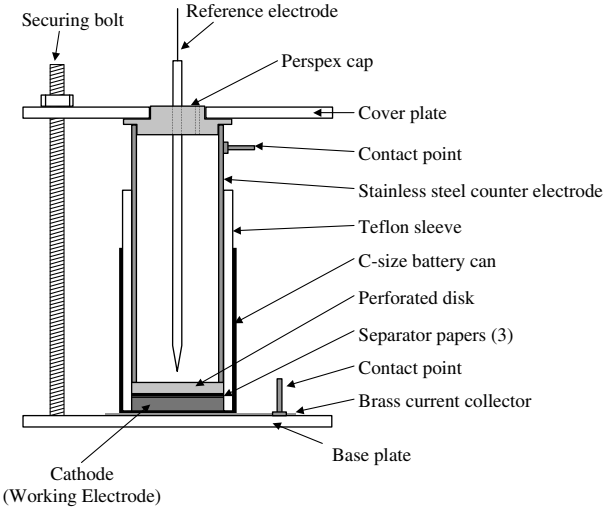

Fig. 1. Schematic diagram of the electrochemical cell.

remove attached particles and three separator papers were placed on top of the sample. A stainless steel piston was then inserted into the can and used to compress the sample mixture (under 1 tonne) to form a compact electrode within the cell. After compaction, the piston was removed from the cell and replaced with a perforated Perspex separator disc and a cylindrical stainless steel counter electrode. The chamber was then filled with ~15 ml of 9 M KOH electrolyte and the Perspex cap inserted. The cell was then mounted between the cover and baseplate, on top of the brass current collector, and held in place with three securing bolts that were each tightened to a torque of 0.75 nm to ensure a uniform pressure. A Hg/HgO reference electrode was inserted into the completed cell, which was then left to equilibrate for one hour prior to discharge.

2.3. *Discharge regime*

Separate cells were prepared from the same composite electrode mixture for the linear sweep voltammetry and step potential electrochemical spectroscopy (SPECS) experiments. In the SPECS experiments, sequential 10 mV cathodic steps, with a 2 h rest period after each step, were applied from the open circuit voltage of the cell until discharge was complete (< -0.4 V vs Hg/HgO). The resulting current after each step was recorded as a function of time. Linear sweep voltammetry was also performed at a rate of 1.39 μV s^{-1}, corresponding to the same discharge rate as the SPECS experiments, also from the open circuit voltage of the cell to -0.4 V. All experiments were conducted at a temperature of 22 ± 1 °C.

3. Results and discussion

Transient techniques in electrochemistry have been used extensively to examine kinetic features of the system under study. Of particular use in the study of solid intercalation electrode systems are techniques such as the potentiostatic [33, 34] or galvanostatic [35] intermittent titration technique (PITT or GITT, respectively) in the sense that they provide both thermodynamic and kinetic information about the electrode system under study. Step potential electrochemical spectroscopy (SPECS) can be considered as an alternative name for a PITT experiment. The basis of these experiments is that they fractionally discharge the electrode under study by the application of either a small potential step or current pulse, and then monitor either current flow or voltage change, respectively. Interpretation of the transient current or voltage signal allows for a kinetic analysis of the system since these can be related back to the physical processes occurring in the electrode. If the transient signal is monitored for a sufficiently long time it will reach an equilibrium value; i.e., zero current or constant voltage. Determining the conditions under which these equilibrium values occur, as a function of depth of discharge, thus provides us with the requisite thermodynamic data.

In terms of the manganese dioxide electrode, PITT or SPECS has been used previously by a number of authors [8, 21, 36–42]. One of the great advantages of this technique, of particular relevance to the study of the manganese dioxide electrode, is that by judicious choice of the voltage step size, individual processes occurring within the electrode can be resolved [8]. With at least three individual processes occurring during homogeneous reduction, a small step size is necessary to obtain unbiased data.

In terms of the kinetic (i–t) data arising from each voltage step, conventional analysis to determine a diffusion coefficient (i–$t^{-1/2}$) [43] has been shown to be only appropriate for very short time periods after the potential step [36], thus indicating the inherent complexity of the system in terms of both a physical model and possible contributions from multiple reduction processes. In the search for an appropriate kinetic model, Hong et al. [21] compared linear semi-infinite, spherical, and double plane models for their i–t data. They found the double plane model described the step potential discharge of EMD most closely; however, none of the models fit the experimental data particularly well. The models could be made to fit the early stages of the step, with later stages poorly described, or vice versa. Despite the fact that they used a relatively small voltage step (15 mV), and hence expected good resolution, the poor fit of their models suggests that there might be contributions from multiple processes occurring.

As has been mentioned, a number of previous studies [8, 15–17, 20–22] have demonstrated the existence of several energetically different processes during EMD reduction. Figure 2 shows a linear sweep voltammogram of our EMD sample recorded at 1.39 μV s^{-1}, corresponding to the same discharge rate as our SPECS experiments. Each individual process occurring during homogeneous reduction was resolved and characterized using the following expression derived from the Nernst equation

$$\frac{dQ}{dE} = \frac{-\frac{n^2MF^2}{RT}\exp\left(\frac{nF}{RT}(E-E^{o})\right)}{1+\exp\left(\frac{nF}{RT}(E-E^{o})\right)} \qquad (2)$$

where Q is the charge passed during discharge (C g^{-1}), E is the electrode voltage, E^{o} is the mean voltage for the process, n can be regarded as an indicator of electrode kinetics (large n implies a facile process, while a small n suggests sluggish kinetics), M is the number of moles associated with the particular process, and the remaining symbols have their usual meaning. The method and assumptions made during the derivation of Equation (2) appear elsewhere [44]; however, for the sake of completeness, the main assumptions are that reduction is homogeneous and occurs completely in the solid state, the activities of H_2O and OH^- can essentially be ignored, and that the potential of the solid is determined by the mole fractions of Mn^{3+} and Mn^{4+}. By solving for n, M and E^{o} using least squares regression, six

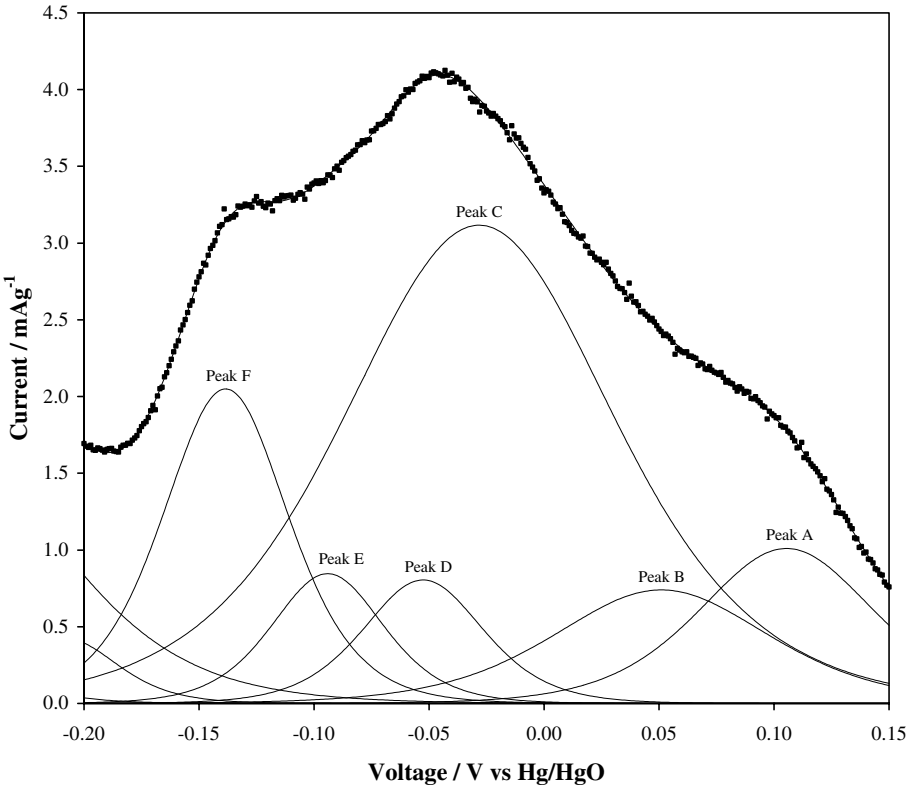

Fig. 2. Deconvolution of the EMD voltammogram.

processes (each with their own individual n, M and E^{o} values) were resolved over the voltammogram range. While this number of processes exceeds the numbers reported previously [7, 15–17, 20–22], it is in no way unrealistic given the preponderance manganese dioxide has for forming intergrowth structures [45]. Nevertheless, identifying the origin of these processes in terms of material structure is still a topic for debate. Because the deconvoluted peaks overlap, the total current that flows must have contributions from multiple processes. Figure 3 shows the contribution of each process to the total current as a function of potential.

As with linear sweep voltammetry, SPECS data should also be made up of contributions from these processes. Therefore, Figure 3 also allows the estimation of the contribution each process makes to the overall current that flows after each potential step. Thus, the overall SPECS curve can be modelled by treating it as the sum of the curves for each process. Throughout this analysis, a spherical model [21] has been assumed for each process, as shown in Equation (3). A spherical model was used because of recent TEM results which showed that EMD morphology consists of approximately spherical grains [9].

$$i = \frac{2FAD\Delta C}{a}\sum_{n=1}^{\infty}\exp\left(-\frac{n^2\pi^2 Dt}{a^2}\right) \tag{3}$$

where i is the current density (A g^{-1}), A is the electrochemically active surface area of the sample (cm^2 g^{-1}), D is the diffusion coefficient (cm^2 s^{-1}), ΔC is the change in concentration over the potential step (mol cm^{-3}), a is the radius of a particle (cm), and t is time (s). The boundary conditions used in the derivation of Equation (2) are described in Ref. [21]. By combining these variables to produce two fitting parameters, P_1 and P_2, Equation (2) can be simplified to

$$i = P_1\sum_{n=1}^{\infty}\exp\left(-n^2P_2t\right) \tag{4}$$

where

$$P_1 = \frac{2FAD\Delta C}{a} \quad \text{and} \quad P_2 = \frac{\pi^2 D}{a^2} \tag{5}$$

Experimental discharge data can be fit with Equation (3) by solving for P_1 and P_2 using least squares regression. P_1 and P_2 are then used in Equation (6) to calculate $A\sqrt{D}$. The particle radius does not need to be determined as it is cancelled out in the division of P_1^2 by P_2.

$$A\sqrt{D} = \sqrt{\frac{P_1^2}{P_2}\cdot\left(\frac{\pi}{2F\Delta C}\right)^2} \tag{6}$$

It was assumed that for each process, the diffusion coefficient (D) and particle radius (a) remained constant, and consequently that the P_2 term also remained constant.

The contribution to the total charge from each process was determined by the area under the experimental i–t data, multiplied by the fractional contribution of the specific process at the step potential given by Figure 3. The experimental data was then solved for P_1

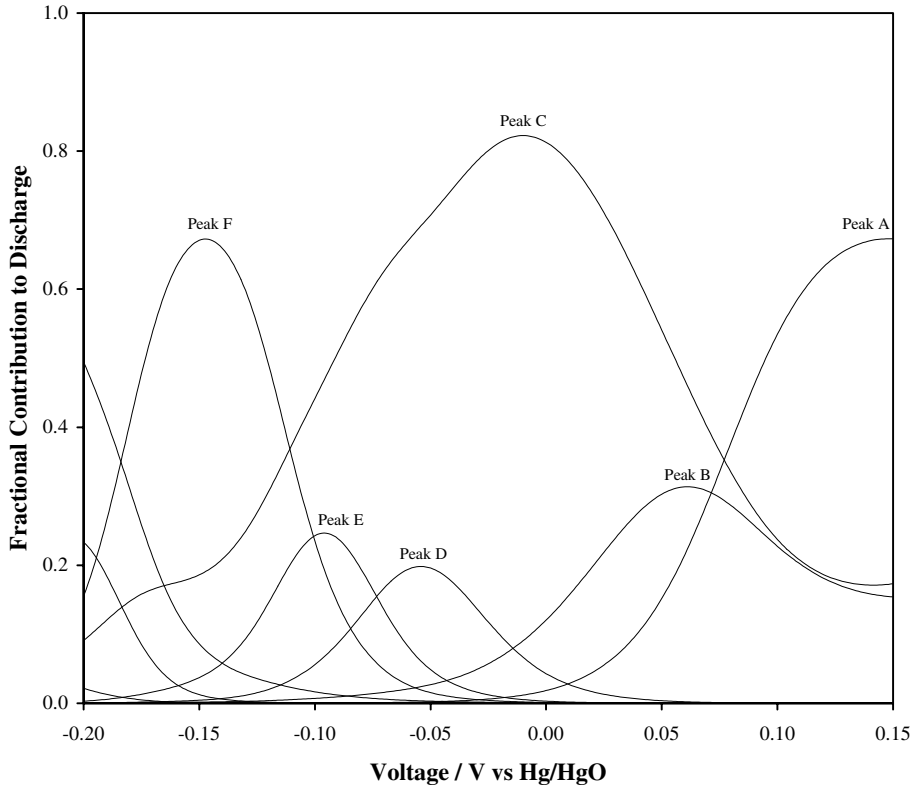

Fig. 3. Fractional contribution to discharge as a function of potential.

and P_2 for all steps simultaneously with the areas under each curve (i.e., the charge) for each process held constant. Figure 4 shows typical results from three different potentials. At high potentials (Figure 4(a)), the discharge is made up of contributions from processes A, B and C only. At mid-range potentials (Figure 4(b)), the discharge is made up almost entirely by process C, with processes A, B and D making small contributions. At low potentials (Figure 4(c)), the contributions by processes E and F have increased, while process C has decreased. The sum of these processes is in good agreement with the experimental data with some deviation where the slope changes rapidly (at $\sim$500 s).

Figures 5 and 6 show the calculated $A\sqrt{D}$ for the six processes as a function of potential and of degree of reduction, respectively. Since the diffusion coefficient is assumed to be constant for each process, the arch-like shape exhibited by the curves can possibly be attributed to changes in the electrochemically active surface area. Each process can be thought of as a distribution of energetically different sites about the peak potential. At the beginning of the peak, only a small proportion of sites will be of the required energy level to be reduced and hence only a fraction of the total surface area is electrochemically active. As most of the sites lie near the peak potential, the electrochemically active surface area will reach a maximum. As the potential moves past the peak, fewer sites are available and hence the active area decreases.

As mentioned before, the structure of EMD is quite complex, and assigning a series of $A\sqrt{D}$ values to a particular component of the structure can be quite prone to speculation rather than hard scientific facts. Nevertheless, the higher voltage processes (A and B) have been reported to involve reduction of Mn^{4+} ions on or near the EMD surface, and/or near defects within the structure. This assignment seems appropriate given the anticipated higher potential energy of Mn^{4+} ions in these locations. The fact that process A has a relatively high $A\sqrt{D}$ value (maximum of 2.3×10^{-2} cm^3 s$^{-1/2}$ g^{-1}) relates to the facility of the diffusing species through these sites. For instance, reduction of surface Mn^{4+} ions could involve lateral or surface diffusion which would tend to be faster given the ready availability of protons in the electrolyte at the surface. Furthermore, reduction of Mn^{4+} ions near higher energy structural defects such as cation vacancies, could be expected to be a facile process due to the fact that the cation vacancies can (at least conceptually) enhance proton mass transport through the structure. Process C, which is clearly the greatest contributor to discharge capacity (51%), occurring at intermediate voltages, has been assigned previously to the reduction of Mn^{4+} ions located in ramsdellite domains within the γ-MnO_2 structure. This process has a maximum $A\sqrt{D}$ value of 1.7×10^{-3} cm^3 s$^{-1/2}$ g^{-1} which is comparable to literature values of $\sim 10^{-3}$ cm^3 s$^{-1/2}$ g^{-1} [30]. The processes occurring at lower voltages during discharge tend to be substantially overlapped. Previously, the processes occurring in this voltage range were assigned to the reduction of Mn^{4+} ions in pyrolusite domains, due to the high thermodynamic stability of this pure

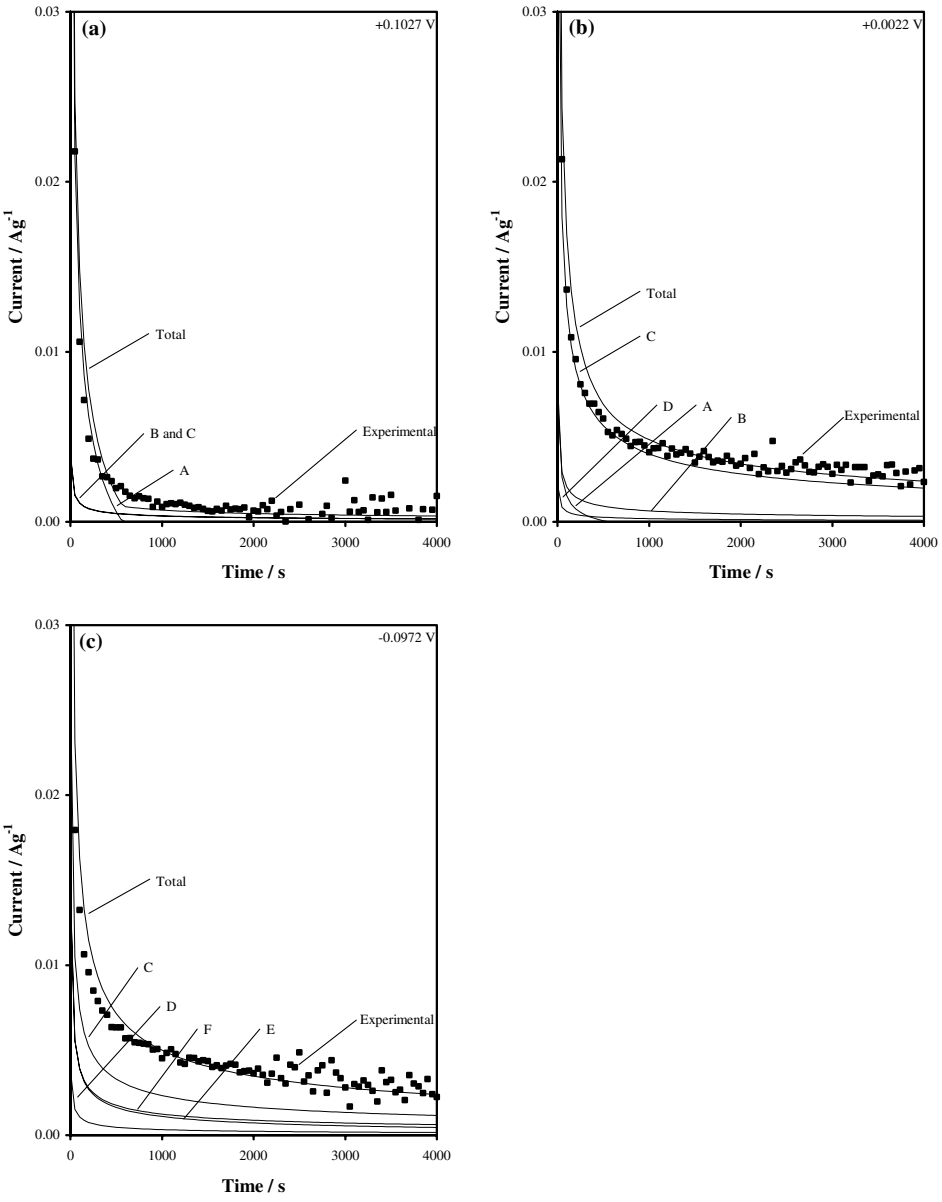

Fig. 4. SPECS discharge curves showing components at potentials (a) +0.1027 V, (b) +0.0022 V, and (c) −0.0972 V.

manganese dioxide crystal phase. However, with considerable TEM evidence to suggest that there are other manganese dioxide phases or domains present in EMD [45], it is possible that they too are being reduced in this lower voltage range. What is significant is that while the maximum $A\sqrt{D}$ for processes B, D and E are relatively low (4.0×10^{-4}, 4.6×10^{-4} and 4.8×10^{-4} $cm^3\ s^{-1/2}\ g^{-1}$, respectively), process F has an $A\sqrt{D}$ value comparable with the fastest higher voltage processes (1.8×10^{-2} $cm^3\ s^{-1/2}\ g^{-1}$. Given that the solid state reduction of pyrolusite is kinetically slow, preferring instead to undergo reduction via a dissolution-precipitation mechanism [46], this facile lower voltage process may be associated with the reduction of Mn^{4+} ions in larger tunnels within the structure [45]. Alternatively, it may be an artefact related to a change in the EMD reduction mechanism away from solid state reduction. It has been shown that at high degrees of discharge ($r+\Delta > 0.8$ in Equation (1)) corresponding to low electrode voltages, where the Mn^{3+} activity in the solid increases, EMD, in a similar fashion to pyrolusite, undergoes dissolution to form a soluble Mn^{3+} intermediate [17]. Depending on the electrode potential the soluble Mn^{3+} can either be re-precipitated as a distinct solid Mn^{3+} species (relatively high voltage), or reduced to Mn^{2+} which precipitates almost immediately as $Mn(OH)_2$ (low voltages). In this latter case, the changing discharge mechanism may have influenced the i–t measurement.

4. Conclusions

In this work, the $A\sqrt{D}$ values for the processes that take place during homogeneous reduction of EMD have been calculated. The contributions of these processes to the

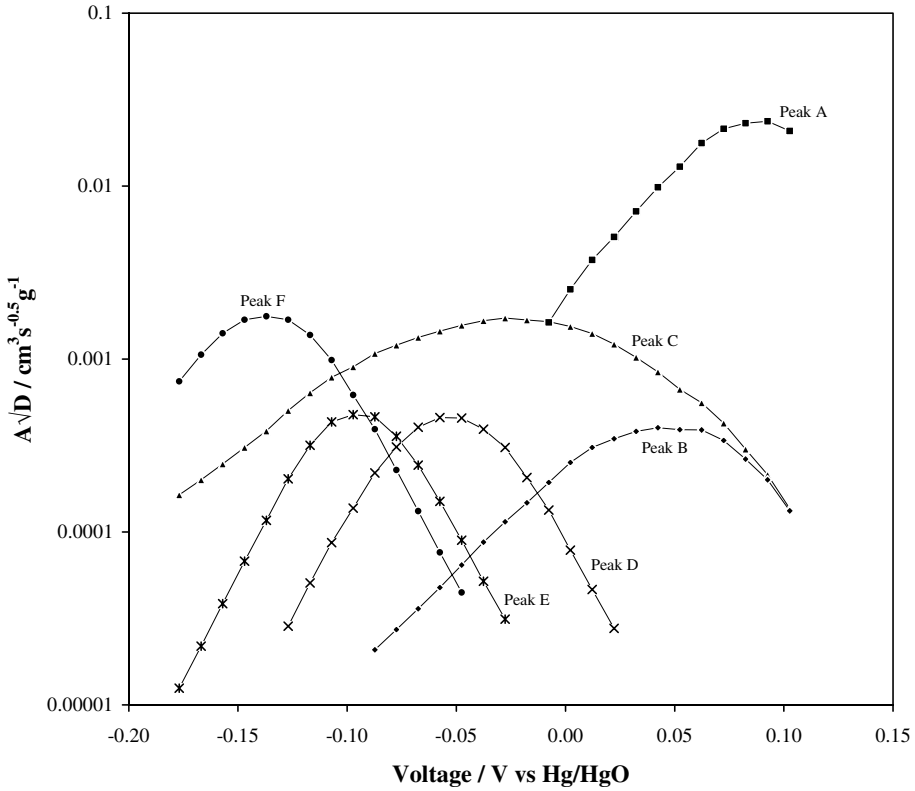

Fig. 5. $A\sqrt{D}$ of individual processes as a function of potential.

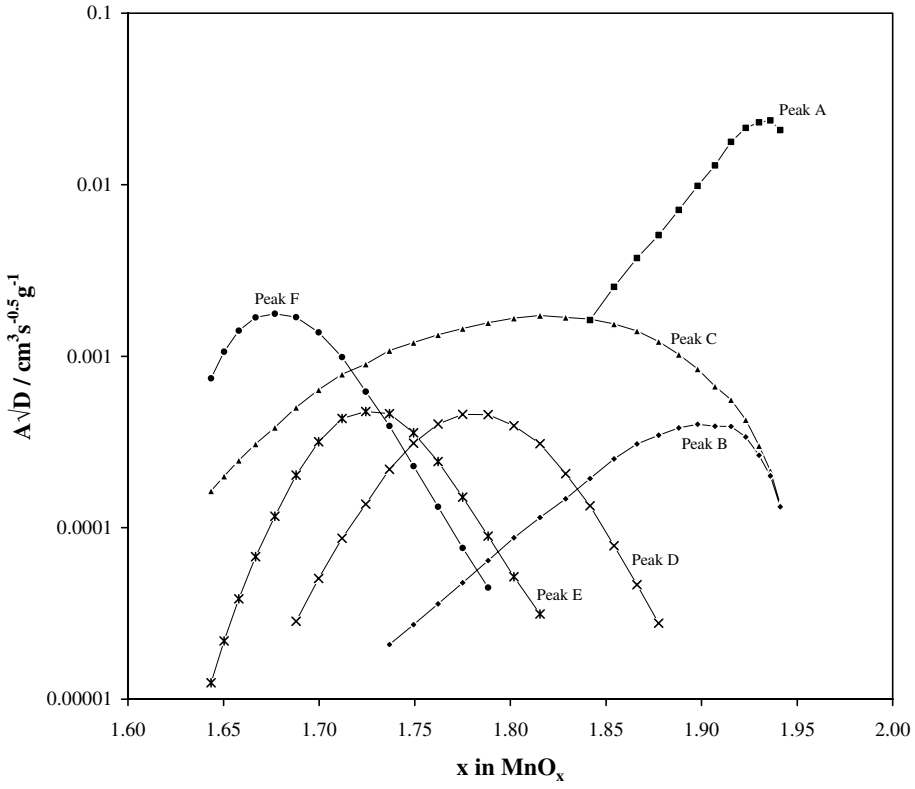

Fig. 6. $A\sqrt{D}$ of individual processes as a function of degree of reduction (x in MnO_x).

total discharge were determined as a function of potential by the deconvolution of a linear sweep voltammogram. Using a spherical particle model to describe the discharge of each process, the sum of these curves was fit to the experimental data. Plots of $A\sqrt{D}$ as a function of degree of reduction show an arch-like shape that was attributed

to changes in the electrochemically active surface area. The determined values of $A\sqrt{D}$ are also compatible with previously reported data, although in this work we have deconvoluted the homogeneous discharge into contributions from each individual process.

Acknowledgements

The authors would like to acknowledge the financial support for this project made available by the Australian Research Council (LP0346943) and Delta EMD Australia Pty Limited. Dr. Rodney Williams from Delta EMD is also acknowledged for many related technical discussions.

References

1. R.G. Burns and V.M. Burns, in 'Proceedings of the Manganese Dioxide Symposium' (edited by A. Kozawa and R. J. Brodd), Vol. 1, Cleveland (1975) p. 306.
2. R.G. Burns and V.M. Burns, in 'Proceedings of the Manganese Dioxide Symposium' (edited by B. Schumm, H. M. Joseph and A. Kozawa), Vol. 2, Tokyo (1980) p. 97.
3. R. Giovanoli. in I.M. Varentsov and G. Grasselly (Eds), 'Geology and Geochemistry of Manganese' Vol. 1, (Akademiai Keadó, Budapest, 1980), pp. 159.
4. P.M. De Wolff, *Acta Cryst.* **12** (1959) 341.
5. P. Ruetschi, *J. Electrochem. Soc.* **131** (1984) 2737.
6. P. Ruetschi, *J. Electrochem. Soc.* **135** (1988) 2657.
7. P. Ruetschi and R. Giovanoli, *J. Electrochem. Soc.* **135** (1988) 2663.
8. Y. Chabre and J. Pannetier, *Prog. Solid State Chem.* **23** (1995) 1.
9. A.H. Heuer, A.Q. He, P.J. Hughes and F.H. Feddrix, *ITE Lett. Batt., New Tech. Med.* **1** (2000) 926.
10. A. Kozawa and J.F. Yeager, *J. Electrochem. Soc.* **112** (1965) 959.
11. A. Kozawa and R.A. Powers, *J. Electrochem. Soc.* **113** (1966) 870.
12. A. Kozawa and R.A. Powers, *Electrochem. Tech.* **5** (1967) 535.
13. A. Kozawa and R.A. Powers, *J. Electrochem. Soc.* **115** (1968) 122.
14. A. Kozawa and J.F. Jeager, *J. Electrochem. Soc.* **115** (1968) 1003.
15. S.W. Donne, G.A. Lawrance and D.A.J. Swinkels, *J. Electrochem. Soc.* **144** (1997) 2949.
16. S.W. Donne, G.A. Lawrance and D.A.J. Swinkels, *J. Electrochem. Soc.* **144** (1997) 2954.
17. S.W. Donne, G.A. Lawrance and D.A.J. Swinkels, *J. Electrochem. Soc.* **144** (1997) 2961.
18. J.M. Amarilla, F. Tedjar and C. Poinsignon, *Electrochim. Acta* **39** (1994) 2321.
19. X. Xi, L. Hong and C. Zhenhai, *J. Electrochem. Soc.* **136** (1989) 266.
20. D.A.J. Swinkels, K.E. Anthony, P.M. Fredericks and P.R. Osborn, *J. Electroanal. Chem.* **168** (1984) 433.
21. Z. Hong, C. Zhenhai and X. Xi, *J. Electrochem. Soc.* **136** (1989) 2771.
22. W. Bowden, K. Brandt, J.J. Cervera, H.S. Choe, R.A. Sirotina and J. Sunstrom, US Patent 6,509,117 (2003).
23. J.P. Gabano, J. Seguret and J.F. Laurent, *J. Electrochem. Soc.* **117** (1970) 147.
24. A.B. Scott, *J. Electrochem. Soc.* **107** (1960) 941.
25. H. Laig-Hörstebrock, *J. Electroanal. Chem.* **180** (1984) 599.
26. S. Atlung and T. Jacobsen, *Electrochim. Acta* **21** (1976) 575.
27. M.A. Malati, M.W. Rophael and I.I. Bhayat, *Electrochim. Acta* **26** (1981) 239.
28. M.W. Rophael and M.A. Malati, *Atomkernenergie* **25** (1975) 231.
29. H. Kahil, F. Dalard, J. Guitton and J.P. Cohen-Addad, *Surf. Tech.* **16** (1982) 331.
30. R.P. Williams, *Ph. D Thesis*, University of Newcastle. (1996).
31. K.J. Vetter and N. Jaeger, *Electrochim. Acta* **11** (1966) 401.
32. S. Brunauer, P.H. Emmett and E. Teller, *J. Am. Chem. Soc.* **60** (1938) 309.
33. C.J. Wen, B.A. Boukamp, R.A. Huggins and W. Weppner, *J. Electrochem. Soc.* **126** (1979) 2258.
34. A.H. Thompson, *J. Electrochem. Soc.* **126** (1979) 608.
35. W. Weppner and R.A. Huggins, *Ann. Rev. Mater. Sci.* **8** (1978) 269.
36. Y.P. Chabre, *J. Electrochem. Soc.* **138** (1991) 329.
37. W. Bowden, K. Brandt, J.J. Cervera, H.S. Choe, R.A. Sirotina and J. Sunstrom, US Patent 6,440,181 (2002).
38. W. Bowden, R.A. Sirotina and S. Hackney, *ITE Letters* **1**(6) (2000) B27.
39. W. Bowden, C.P. Grey, S. Hackney, X.Q. Yang, Y. Paik, F. Wang, T. Richards and R. Sirotina, *ITE Letters* **3**(3) (2002) B1.
40. W. Bowden, C.P. Grey, R. Sirotina, T. Richards, F. Wang and Y. Paik, *ITE Letters* **4**(2) (2003) B1.
41. W. Bowden, S. Hackney and R. Sirotina, *ITE Letters* **4**(1) (2003) B1.
42. Y. Paik, W. Bowden, T. Richards, R. Sirotina and C.P. Grey, *J. Electrochem. Soc.* **151** (2004) A998.
43. A.J. Bard and L.R. Faulkner, *Electrochemical Methods – Fundamentals and Applications* (John Wiley and Sons, New York, 1980).
44. G.J. Browning and S.W. Donne, *J. Appl. Electrochem.* in press (2005).
45. S. Turner and P.R. Buseck, *Nature* **304** (1983) 143.
46. A.P. Malloy, G.J. Browning and S.W. Donne, *J. Coll. Inter. Sci.* In press (2005).